Facile Synthesis and High Rate Capability of Silicon Carbonitride/Boron Nitride Composite with a Sheet-Like Morphology

Lamuel David, Samuel Bernard, Christel Gervais, Philippe Miele, Gurpreet Singh

Facile Synthesis and High Rate Capability of Silicon Carbonitride/Boron Nitride Composite with a Sheet-Like Morphology

Lamuel David[1], Samuel Bernard[2], Christel Gervais[3], Philippe Miele[2], and Gurpreet Singh[1]*

[1]Mechanical and Nuclear Engineering Department, Kansas State University, Manhattan, Kansas, 66506-United States

[2]IEM (Institut Europeen des Membranes), UMR 5635 (CNRS-ENSCM-UM2), Universite Montpellier 2, Place E. Bataillon, F-34095, Montpellier, France

[3]Sorbonne Universités, UPMC Univ Paris 06, CNRS, Collège de France, UMR 7574, Chimie de la Matière Condensée de Paris, F-75005, Paris, France

*E-mail: gurpreet@ksu.EDU Tel.: +1-785-532-7085 Fax: +1-785-532-7057

ABSTRACT

We report synthesis of a sheet-like composite composed of hexagonal boron nitride (or BN) chemically integrated with silicon carbonitride (SiCN) matrix *via* a simple pyrolysis route. The composite offers several unique features such as improved electrical conductivity, high-temperature oxidation resistance (at 1000 °C), and high electrochemical activity toward Li-ions generally not observed in SiCN or boron doped SiCN. Tested as electrode in Li-ion half-cell, SiCN/BN show charge capacity of ~517 mAh g^{-1} at 100 mA g^{-1} and 283 mAh g^{-1} at 2400 mA g^{-1} with respect to total weight of electrode. Additionally, a stable charge capacity of ~401 mAh g^{-1} at 100 mA g^{-1} is retained even after continuous operation for 1000 cycles at 1600 mA g^{-1}. Chemical characterization of the composite suggests that addition of BN to polysilazane in moderate amounts (~10 wt%) and subsequent pyrolysis resulted in an increased free-carbon

content in the amorphous SiCN phase, which exceeded the percolation limit, leading to the improved electrical conductivity and Li-reversible capacity.

Keywords: graphene, nanosheets, polymer-derived ceramics, anode, lithium ion battery, 2-D materials.

INTRODUCTION

Powering of electric vehicles or next generation wearable electronic devices that run on Li-ion battery (LIB) technology will require new electrode materials beyond the traditional graphite anode because of its poor rate capability and low charge capacity (theoretical charge capacity approximately 372 mAh g^{-1}).[1-7] Desired characteristics of next-generation LIB system include high power and energy density, improved safety, long life, and lightweight. [1-2, 8] Research has shown that silicon (Si) anodes can drastically increase the capacity of existing LIB by more than 30%. [9-11] Unfortunately, however, Si experiences huge volume changes during charge/discharge cycles and has poor electrical conductivity that generally leads to poor rate capability.[12-13] Although, nanoengineered Si-based materials (such as nanowires, nanoparticles and hollow nano-spheres) that can sustain large mechanical strains with minimal capacity degradation have shown promise in laboratory experiments, a practical and cost-effective solution is yet to be realized.[14-26]

Among other Si-based materials for LIB anodes, silicon-based polymer-derived ceramics (or PDCs) rich in carbon have shown high specific capacity even at high current densities.[27-39] These ceramics are lightweight (density ~1.8 to 2.2 $g.cm^{-3}$), chemically inert, stable at high temperatures, and readily synthesized through direct pyrolysis of single-source polymeric precursors. Two main types of PDCs, SiCO (silicon oxycarbide) and SiCN (silicon carbonitride), have gained attention because their Li discharge capacity is nearly 3 times the discharge capacity

of commercial graphite anode.[28-30, 32-38] This high capacity is derived from the particular structure of PDCs, which consists of a three-dimensional network of silicon, carbon and nitrogen (or oxygen for SiCO) atoms and excess disordered carbon (or free carbon phase) that generally provides majority of active sites for reversible adsorption of lithium ions.[34] However, cycling stability and efficiency of polysilazane-derived SiCN is considerably lower than SiCO anode. SiCN generally suffers from very high first cycle loss of Li (up to 70% in certain cases) [29, 31] and has low electrical conductivity that brings down its reversible capacity and rate capability to values similar or worse than commercial graphite after only a few initial cycles.[35-36] Research has shown that some of these weaknesses can be addressed by changing the pyrolysis conditions (such as extended heat treatment), altering the polymeric precursor type (e.g., polysilylcarbodiimide is preferred over polysilazane) or, by introducing a suitable quaternary element, such as boron or aluminum, [40-46] at molecular scale. In previous work, precursor-derived amorphous Si(B)CN ceramics showed improved electric property (up to 4 orders of magnitude higher conductivity than SiCN) and superior electrochemical performance.[46, 47] In addition, composites made of SiCN matrix with filler phases comprised of carbon nanotubes (CNTs),[48] graphite,[49] and carbon nanofiber[50] have been shown to improve electrical conductivity and resistance to mechanical cracking. However, rate capability and cycling stability of Si(B)CN and SiCN-based nanocomposite electrodes remain inferior to polymer-derived SiCO or other nanocomposite electrodes currently under investigation. One reason for this inferiority could be the presence of Si, C, N, O danglings bonds which may form Li irreversible phases resulting in high first cycle loss. For precursor-derived Si(B)CN, it could be the limited amounts of B that is ultimately retained in the pyrolyzed ceramic. Therefore, based on improved electrochemical performance of Si(B)CN ceramics compared to SiCN ceramics, we conclude that introduction of

higher quantities of boron as (nano) sheets or (nano) particles in the SiCN network is a logical parallel step toward the improvement of electrochemical performance. Sheet or particle-like morphology is expected to improve overall accessibility for Li ions in the electrode during successive charge/discharge cycles.

We synthesized a SiCN/BN composite by functionalizing hexagonal boron nitride (h-BN, expressed here as BN) sheets with a commercial off-the-shelf polysilazane precursor, followed by pyrolysis at 1000 °C. We observed that preparation of SiCN/BN composite with a sheet-like morphology provided a unique opportunity to tailor the nitrogen bonds with boron and also increased free carbon content in the SiCN matrix, thereby, improving its electrical conductivity by orders of magnitude compared to boron-free SiCN ceramics. These changes in the molecular structure of the final ceramic yielded a material with excellent electrochemical stability even at high current densities. Composites made of SiCN matrix and precursor-derived BN (SiCN/BNF) and powdered boron (SiCN/BP) as filler phase were also prepared in order to extrapolate and highlight the distinctive chemistry that governs high capacity in SiCN/BN.

MATERIALS AND INSTRUMENTATION

Boron nitride (99.9%) was purchased from Sigma Aldrich. Poly (ureamethylvinyl)silazane (commercial name: Ceraset) was obtained from Clariant Corporation. All materials were used as received without further purification.

Scanning electron microscopy (SEM) of the synthesized material was carried out on a Carl Zeiss EVO MA10 system with incident voltage of 5 kV-30 kV. Transmission electron microscopy (TEM) images were digitally acquired by use of a Phillips CM100 operated at 100 kV. Surface chemical composition was studied by X-ray photoelectron spectroscopy (XPS, PHI Quantera

SXM) using monochromatic Al Kα X-ray radiation. ^{11}B MAS NMR spectra were recorded at 11.7 T on a Bruker Avance500 wide-bore spectrometer operating at 160.47 MHz, using a Bruker 4 mm probe and a spinning frequency of the rotor of 12 kHz. Spectra were acquired using a spin-echo θ-t-2θ pulse sequence with θ=90° to overcome problems of probe signal. The t delay (83 μs) was synchronized with the spinning frequency and recycle delay of 1s was used. Chemical shifts were referenced to $BF_3(OEt)_2$ (δ=0 ppm). The FTIR spectra were collected using Thermo-Nicolet Nexus 870FT-IR spectrometer. FTIR samples were prepared by mixing ~1 wt% of the finely powdered sample with FTIR grade KBr powder. Phase evolution was characterized by using Bruker powder X-ray diffractometer (Madison, WI) operating at room temperature, with CuKα radiation and nickel filter. The pyrolyzed samples were finely crushed with mortar and pestle and laid on the palette for analysis. Thermogravimetric analysis was performed using Shimadzu 50 TGA (Columbia, MD) (limited to 1000° C). Sample weighing, ~2.5 mg, was heated in a platinum pan at a rate of 10 °C min^{-1} in air flowing at 10 mL min^{-1}.

PREPARATION OF SiCN/BN, SiCN/BNF, SiCN/BP

SiCN/BN: Chemical modification of Polyureasilazane (commercial name: Ceraset) was performed using commercially obtained BN (99.9%) nanosheets from Sigma Aldrich™. 1 g of BN (sonicated in propanol and dried) was mixed with 10 mL of polyureasilazane and stirred for 12 h at room temperature. Subsequently the mixture was cross-linked at 250 °C (heating rate 100 °C h^{-1}) for 180 min to obtain a white powder. The cross-linked powder was then pyrolyzed in N_2 atmospheres at 1000 °C in a tube furnace to obtain an amorphous black powder termed as SiCN/BN.

SiCN/BNF and SiCN/BP specimens: Similar procedure was followed as conducted for SiCN/BN preparation with the exception that instead of commercially obtained BN, the following boron modifiers were added to polyureasilazane: cross-linked BN polymeric precursor synthesized using procedure from literature[51-57] for synthesizing SiCN/BNF and commercially obtained boron powder from Sigma Aldrich for SiCN/BP.

PREPARATION OF PAPER ELECTRODE

10 mL colloidal suspension of GO (graphene oxide) in 1:1 (v/v) water was made by sonication for 10 minutes. GO was synthesized using Hummer's method.[58] 60 wt% active material (SiCN/BN, SiCN/BNF or SiCN/BP) in 10 mL of isopropanol (ISP) was added to this solution and the solution was further sonicated for 60 min. When creation of the composite suspension was complete, it was filtered by vacuum filtration through a 10 μm filter membrane. Composite paper was carefully removed from the filter paper and dried. This dry paper then underwent reduction by heat treatment in a tube furnace at 500 °C under flowing argon gas for 2 h. The thermal reduction process resulted in conversion of GO to rGO (reduced graphene oxide) with approximately 50-60% weight loss. The thermally reduced composite papers consisted of approximately 20 wt.% rGO.

COIN CELL ASSEMBLY

Half-cell batteries were made by punching a 14.3 mm diameter circle from the paper for use as working electrode. A few drops of electrolyte solution of 1 M $LiPF_6$ (Alfa Aesar^{TM}) dissolved in (1:1 v/v) dimethyl carbonate: ethylene carbonate (ionic conductivity 10.7 mS cm^{-1}) was used. A 19 mm diameter glass separator soaked in electrolyte was placed between the working electrode and pure lithium metal (14.3 mm diameter), which acted as a counter electrode. Washer, spring,

and a top casing were placed on top to complete the assembly before crimping. The entire procedure was conducted out in an Ar-filled glovebox.

Electrochemical performance of assembled coin cells was tested using a multichannel BT2000 Arbin^{TM} test unit sweeping 2.5 V to 10 mV versus Li/Li^{+} using the following cycle schedule: (a) Asymmetric mode: Li was inserted at 0.1 A g^{-1} (with respect to total electrode weight), while the extraction was performed at increasing current densities of 100, 200, 400, 800, 1600 and 2400 mA g^{-1} for five cycles each, and returning to 100 mA g^{-1} for the subsequent 10 cycles. (b) Symmetric mode: Later, all the cells were subjected to symmetric cycling at a current density of 1600 mA g^{-1} for up to 1000 cycles, returning to 100 mA g^{-1} for the last 20 cycles.

RESULTS AND DISCUSSIONS

The schematic in Figure 1 describes the possible reaction mechanism involved in the formation of SiCN/BN composite. We hypothesize that vigorous physical mixing of few-layer thick boron nitride (BN) sheets with liquid polysilazane results in their chemical functionalization, which, upon cross-linking at 300 °C, forms polysilazane/BN polymer composite. With additional heating in N_2 at 1000 °C, polysilazane transforms to SiCN with evolution of H_2, CH_4, and NH_3 forming an integrated SiCN/BN composite with a layered morphology.

Electron microscopy images of as-obtained BN powder and as-synthesized SiCN/BN composite are compared in Figure 2 and Supporting Information Figure S1. TEM and SEM images confirmed a layered and ‘fluffy’ structure of the as-obtained BN, while SiCN/BN composite appeared more dense and compact, although sheet-like morphology of initial BN could still be observed. The selected area electron diffraction (SAED) pattern for SiCN/BN was similar to BN, indicating that BN sheets were intact in the composite. From the SEM images, the average

particle size of SiCN/BN was observed to be approximately (5 to 10) μm. As-pyrolyzed SiCN and SiCN modified with boron particles (i.e., SiCN/BP) and cross-linked polyborazylene (i.e., SiCN/BNF) appeared more irregular with tiny particles decorating big micrometer size particles, as shown in Supporting Information Figure S1(a through e) in a side-by-side comparison.

Top-view and cross-section SEM images of various paper electrodes prepared with rGO (reduced graphene oxide) as conducting support (see Methods section for electrode preparation) are presented in Supporting Information Figure S1 (f through o); the free-standing paper electrode with rGO support had a thickness of approximately 20 to 25 μm. Closer examination showed the paper to be layered with rGO platelets embedded with SiCN/BN particles which had sheet-like morphology.

Further characterization involved X-ray photoelectron spectroscopy (XPS) analysis of SiCN/BN composite as shown in Figure 3(a-b), which revealed distinct peaks from which elemental composition of the final material was confirmed. Survey scans in Supporting Information Figure S2 of SiCN/BN showed the existence of Si, B, N and C elemental peaks rising from valence energy levels for the respective atoms. Atomic percentage of boron in the composite was 6.8%, which is much higher than other boron-doped SiCN.[40] The peak at approximately 190.5 eV for high resolution B 1s in Figure 3b confirmed the presence of B-N bond in the pyrolyzed composite, thereby suggesting successful retention of BN after pyrolysis.[40, 42] High resolution XPS spectrum of C 1s and N 1s for SiCN and SiCN/BP are included in Supporting Information Figure S3. A comparison of C 1s peaks with SiCN/BN revealed that three distinct peaks could be fitted at 283.4, 284.5, and 288 eV attributed to Si-C, C-C, and C-O bonds, respectively. Closer examination of the area under the peaks revealed a higher percentage of C-C bonds (-sp^2 type carbon) in SiCN/BN (0.14 %) compared to 'neat' SiCN (0.04%) and SiCN/BP (0.1%)

specimens. The N 1s spectrum for SiCN/BN specimen could be resolved to Si-N (396.8 eV) and B-N (398.2 eV) while the spectrum for SiCN and SiCN/BP specimens were similar and resolved to two Si-N bonds at (396.8 and 397.1 eV). High-resolution B 1s spectrum (Supporting Information Figure S4) of SiCN/BNF was quite different with an emergence of a weak peak at 192.2 eV. That peak was the only observable peak in SiCN/BP.

The chemical bonds present were also characterized using Fourier Transform Infrared (FTIR) spectroscopy which showed that SiCN/BN and SiCN/BNF had strong BN bond vibrations with no obvious presence of B-O bonding (Supporting Information Figure S5). Peaks ascribed to vinyl groups are C-H vibrations at 3047 cm^{-1} and C-C stretching at 1591 cm^{-1}. Peaks attributed to Si-NH-Si groups are N-H stretching at 3374 cm^{-1} and Si-N vibration at 1160 cm^{-1}. Si-CH_3 characteristic peaks are at 1253 cm^{-1} and methyl vibrations at 2954 and 2896 cm^{-1}. The large peak at 2111 cm^{-1} is attributed to Si-H and small peaks at 805 and 750 cm^{-1} can be assigned to Si-N and Si-C, respectively.[59-63]

Additional characterization of the composite was carried out by use of solid-state NMR (^{11}B), as shown in Figure 3c. ^{11}B solid-state MAS NMR spectra of samples SiCN/BN and SiCN/BNF demonstrated a main signal in the region of tricoordinated boron atoms tentatively simulated with a site at 30 ppm (CQ = 3.0 MHz, η = 0.2) assigned to B-N bonds in planar BN_3 groups within BN graphitic layers. A second small signal at δ_{iso} = 0.6 ppm (no quadrupolar shape) is indicative of the presence of tetragonal BO_4 groups in minor quantity.[54, 55] The ^{11}B spectrum of SiCN/BP showed a shapeless signal centered at 4.5 ppm characteristic of amorphous elemental boron.[64] Chemical characterization of the hybrid matrix involved X-ray diffraction (XRD) to identify crystallinity of the composite material, as shown in Figure 3d. SiCN/BN spectrum was comparable to XRD of as-obtained BN powder spectrum (insert in Figure 3d) with characteristic

002 peak at 28° 2θ, indicating that BN sheets were primarily intact in the amorphous SiCN ceramic matrix. Very weak but similar spectrum was obtained for SiCN/BNF specimen, while SiCN/BP material was featureless in X-ray.

In summary, FTIR and XPS characterization of SiCN/BN composite material suggested the presence of only B-N bonding with little or no evidence of damage to BN sheets upon pyrolysis.[42] While NMR data showed that the boron was tricoordinated as planar BN_3 groups. Amorphous nature of Si-C and Si-N groups and crystalline B-N groups were observed using XRD in SiCN/BN composite material. Results confirmed the structure deduced in Figure 1.

Thermogravimetric analysis (TGA) plots of all materials were compared (see Figure 3e) in order to identify thermal stability. SiCN/BN was extremely stable with no significant weight change even when heated to 1000 °C in flowing air. In contrast, SiCN/BNF composite showed a weight loss attributed to the presence of residual compounds (such as H_2O) in polyborazylene-derived BN (BNF) material. SiCN/BP composites had slight weight gain caused by oxidation of boron into boron oxide.

Four-point surface electrical conductivity of various ceramic specimens was also measured and compared. Data presented in Figure 3f clearly shows that SiCN/BN displayed highest electrical conductive of any specimens at 0.115±0.005 $S.cm^{-1}$, which is as high as doped silicon but lower than the rGO. SiCN/BP demonstrated the next highest electrical conductivity. Increased conductivity of SiCN/BN composite (compared to other PDCs pyrolyzed under similar conditions) [46,47] is attributed to the increased amounts of C-C bonding character in the composite, which was considerably higher as confirmed by the XPS.

Electrochemical behavior of the SiCN/BN/rGO electrode (with approximately 20 wt.% rGO as mechanical support) was studied by cycling it in a half-cell configuration against pure lithium metal. Mass loading of SiCN/BN in the composite paper was confirmed by use of TGA (see Supporting Information Figure S6). Specific capacity values were calculated with respect to total weight of the electrode and mass of active material. Figures 4a and 4b show the charge/discharge profile and differential capacity curves of the SiCN/BN electrode's first two cycles. First cycle discharge and charge capacities were observed to be 891 and 517 mAh g^{-1} with a first cycle loss of 58% at current density of 100 mA g^{-1}. This capacity value is one of the highest reported for polysilazane-based anode materials. [34-38] For example, first reversible capacity of SiCN/BN hybrid composite is better than SiCN annealed at 1000 °C (456 mAh g^{-1}), [36] C-rich SiCN (~263 mAh g^{-1}),[37] SiCN-1300 °C (383 mAh g^{-1}), [38] B-doped SiCN (~100 mAh g^{-1}) [47] and SiCN/graphite (~474 mAh g^{-1}).[49] The differential capacity curve showed first cycle lithiation peaks at 50 mV, 150 mV, a weak plateau at ~700 mV, and a delithiation plateau at ~500 mV. From literature, the peak at 50 mV could be attributed to Li intercalation/adsorption in graphitic carbon[32, 34] and the peak at 150 mV corresponds to interaction of Li in nanovoids or interaction with dangling bonds present at Si and C sites in the ceramic.[32, 37, 47] The plateau at ~700 to 800 mV, present only in the first cycle, originated due to formation of passive solid electrolyte interface (SEI) on graphite. This plateau was common to all electrodes including 'neat' rGO electrode and data from the literature (see Supporting Information Figure S7 for voltage profiles of BP/rGO, and BN/rGO electrodes). The charge/discharge profile and corresponding differential capacity curves of SiCN/BNF/rGO and SiCN/BP/rGO paper electrodes are shown in Supporting Information Figure S8. Lithiation peaks were at 50 mV and ~600 mV with a corresponding delithiation peak at 200 mV (similar to BN/rGO and BP/rGO differential capacity curves). From these results we deduce

that the capacity in SiCN/BN originates primarily from BN enhanced SiCN-based Li intercalation sites while it is not the same in other ceramics that we tested. This is even more evident from the first cycle discharge capacities which were at ~531 mAh g^{-1} and 347 mAh g^{-1} for SiCN/BNF/rGO and SiCN/BP/rGO, respectively. Lower capacity values were observed in subsequent cycles because BN and boron particles have zero or negligible Li cyclability.

With additional cycling (Figure 4c), SiCN/BN/rGO maintained high capacity at 474 mAh g^{-1} (96% of initial capacity retained) which is higher than BN/rGO and SiCN/rGO with charge capacities of 67 and 154 mAh g^{-1}, respectively, after 5 cycles at 100 mA g^{-1}. Current density was gradually increased to 200, 400, 800, 1600 and 2400 mA g^{-1} for each five cycles consecutively. Importantly, SiCN/BN/rGO hybrid composite maintained its reversible capacity of 283 mAh g^{-1} even at 2400 mA g^{-1}. This capacity was 52% of the initial capacity. When the cells were cycled back at 100 mA g^{-1}, all electrodes regained initial charge capacities at 449, 60, and 154 mAh g^{-1} for SiCN/BN/rGO, BN/rGO, and SiCN/rGO, respectively. However, SiCN/BNF/rGO, SiCN/BP/rGO, and BP/rGO performances, shown in Supporting Information Figure S9, were lower than SiCN/BN/rGO. In order to test cell performance during long-term cycling, cells were cycled at 1600 mA g^{-1} during charge and discharge half cycles (see Figure 4d). SiCN/BN/rGO demonstrated stable and high charge capacity of ~62 mAh.g^{-1} than BN/rGO and SiCN/rGO anode at ~25 and 40 mAh g^{-1}, respectively. All electrodes regained most of initial capacity when they were cycled at 100 mA g^{-1} after 1000 cycles. SiCN/BN/rGO was the best performing anode with a charge capacity of ~401 mAh g^{-1} at 100 mA g^{-1} even after symmetric cycling at 1600 mA g^{-1} for 1000 cycles. Summary of the electrochemical data and comparison with recent literature (including graphite[65] and rGO paper electrode[66]) is presented in Table 1. Further, Galvanostatic Intermittent Titration Technique (GITT) was performed to obtain the solid state Li-ion diffusion

coefficient (D_{Li+}) of SiCN/BN electrode (Supporting Figure S10). The acquired D_{Li+} varied between approximately (10^{-10} to 1.4 x 10^{-12}) $cm^2.s^{-1}$ and (3.9 x 10^{-10} to 2.6 x 10^{-11}) $cm^2.s^{-1}$ during the insertion and extraction half, respectively. These values are comparable to SiBCN-CNT (~ 10^{-9} to 10^{-12} $cm^2.s^{-1}$) [47] electrodes but lower than the chemical diffusivity of Li-ion in graphite. [67-68]

High charge capacity of SiCN/BN is attributed to the three-fold advantage associated with the addition of boron to SiCN matrix in the form of BN sheets: (1) possible neutralization of nitrogen atoms by boron. SiCN electrodes with higher nitrogen content typically demonstrates lower electrochemical performance, therefore, increased concentration of boron in SiCN neutralized some of the nitrogen dangling bonds in SiCN during pyrolysis, (2) sheet-like morphology, and (3) significant enhancement in electrical conductivity originating from increased C-C bonds of the SiCN/BN hybrid ceramic matrix compared to other PDC material pyrolyzed under similar conditions.[47]

CONCLUSION

Synthesis of a chemically integrated SiCN/BN layered composite is demonstrated for the first time. The composite shows electrical conductivity similar to conductivity of doped-silicon, which is several orders of magnitude higher than that of 'neat' SiCN prepared under similar conditions. Additionally, unlike its individual constituents, the SiCN/BN composite offers high electrochemical activity and stability toward lithium-ions with charge capacity reaching ~517 mAh g^{-1} at 100 mA g^{-1} and ~283 mAh g^{-1} at 2400 mA g^{-1} with respect to total electrode weight. This behavior is attributed to the increased amount of $-sp^2$ carbon in SiCN phase (observed only in presence of BN) that may have exceeded its percolation limit and provided necessary sites for reversible lithium adsorption. Facile synthesis and improved thermal, electrical and

electrochemical performance of SiCN/BN composite is expected to open new applications for PDCs and 2-D nanomaterial hybrids.

ACKNOWLEDGEMENTS

This research is based on work supported by the National Science Foundation-Chemical, Bioengineering, Environmental, and Transport Systems Division (CBET) under grant no. 1335862 to G. Singh. L.D. Thanks former student Romil and Uriel for assistance with sample preparation. G. Singh thanks Professor G. Sorarù (University of Trento) and Dr. Yigal Blum (SRI International) for their useful insights.

SUPPORTING INFORMATION

SEM, TEM images and electrochemistry data corresponding to SiCN/BN, SiCN/BNF, SiCN/BP ceramic particles and 'neat' BN, BP. GITT data for SiCN/BN electrode. Electrical conductivity data. High resolution XPS C 1s and N 1s spectrum of SiCN, SiCN/BN and SiCN/BP. This information is available free of charge via the Internet at http://pubs.acs.org

REFERENCES

1. Armand, M.; Tarascon, J. M., Building Better Batteries. *Nature* **2008,** *451*, 652-657.
2. Tarascon, J. M.; Armand, M., Issues and Challenges Facing Rechargeable Lithium Batteries. *Nature* **2001,** *414*, 359-367.
3. Goodenough, J. B.; Kim, Y., Challenges for Rechargeable Li Batteries. *Chem. Mater.* **2010,** *22*, 587-603.
4. Arico, A. S.; Bruce, P.; Scrosati, B.; Tarascon, J. M.; Van Schalkwijk, W., Nanostructured Materials for Advanced Energy Conversion and Storage Devices. *Nat. Mater.* **2005,** *4*, 366-377.

5. Choi, N. S.; Chen, Z.; Freunberger, S. A.; Ji, X.; Sun, Y. K.; Amine, K.; Yushin, G.; Nazar, L. F.; Cho, J.; Bruce, P. G., Challenges Facing Lithium Batteries and Electrical Double-Layer Capacitors. *Angew. Chem., Int. Ed.* **2012,** *51*, 9994-10024.
6. David, L.; Bhandavat, R.; Kulkarni, G.; Pahwa, S.; Zhong, Z.; Singh, G. Synthesis of Graphene Films by Rapid Heating and Quenching at Ambient Pressures and Their Electrochemical Characterization. *ACS Appl. Mater. Interfaces* **2013,** *5*, 546-552.
7. Manthiram, A., Materials Challenges and Opportunities of Lithium Ion Batteries. *J. Phys. Chem. Lett.* **2011,** *2*, 176-184.
8. Hu, L.; Xu, K., Nonflammable Electrolyte Enhances Battery Safety. *Proc. Natl. Acad. Sci. U.S.A.* **2014,** *111*, 3205-3206.
9. Park, C. M.; Kim, J. H.; Kim, H.; Sohn, H. J., Li-Alloy Based Anode Materials for Li Secondary Batteries. *Chem. Soc. Rev.* **2010,** *39*, 3115-3141.
10. Zhang, W. J., A Review of the Electrochemical Performance of Alloy Anodes for Lithium-Ion Batteries. *J. Power Sources* **2011,** *196*, 13-24.
11. Wu, H.; Cui, Y., Designing Nanostructured Si Anodes for High Energy Lithium Ion Batteries. *Nano Today* **2012,** *7*, 414-429.
12. Beaulieu, L. Y.; Eberman, K. W.; Turner, R. L.; Krause, L. J.; Dahn, J. R., Colossal Reversible Volume Changes in Lithium Alloys. *Electrochem. Solid-State Lett.* **2001,** *4*, A137-A140.
13. Nadimpalli, S. P. V.; Sethuraman, V. A.; Dalavi, S.; Lucht, B.; Chon, M. J.; Shenoy, V. B.; Guduru, P. R., Quantifying Capacity Loss Due to Solid-Electrolyte-Interphase Layer Formation on Silicon Negative Electrodes in Lithium-Ion Batteries. *J. Power Sources* **2012,** *215*, 145-151.
14. Park, M. H.; Kim, M. G.; Joo, J.; Kim, K.; Kim, J.; Ahn, S.; Cui, Y.; Cho, J., Silicon Nanotube Battery Anodes. *Nano Lett.* **2009,** *9*, 3844-3847.
15. Song, T.; Xia, J.; Lee, J. H.; Lee, D. H.; Kwon, M.-S.; Choi, J.-M.; Wu, J.; Doo, S. K.; Chang, H.; Il Park, W. et al. , Arrays of Sealed Silicon Nanotubes as Anodes for Lithium Ion Batteries. *Nano Lett.* **2010,** *10*, 1710-1716.
16. Kasavajjula, U.; Wang, C.; Appleby, A. J., Nano- and Bulk-Silicon-Based Insertion Anodes for Lithium-Ion Secondary Cells. *J. Power Sources* **2007,** *163*, 1003-1039.

17. Liu, B.; Soares, P.; Checkles, C.; Zhao, Y.; Yu, G., Three-Dimensional Hierarchical Ternary Nanostructures for High-Performance Li-Ion Battery Anodes. *Nano Lett.* **2013,** *13*, 3414-3419.
18. Ruvinskiy, P.; Barsukov, I. V.; Mashtalir, O.; Reid, C. M.; Wu, J. J.; Gogotsi, Y., Nano-Silicon Containing Composite Graphitic Anodes with Improved Cycling Stability for Application in High Energy Lithium-Ion Batteries. *ECS J. Solid State Sci. Tech.* **2013,** *2*, M3028-M3033.
19. McDowell, M. T.; Lee, S. W.; Nix, W. D.; Cui, Y., 25th Anniversary Article: Understanding the Lithiation of Silicon and Other Alloying Anodes for Lithium-Ion Batteries. *Adv. Mater.* **2013,** *25*, 4966-4984.
20. Kim, H.; Seo, M.; Park, M. H.; Cho, J., A Critical Size of Silicon Nano-Anodes for Lithium Rechargeable Batteries. *Angew. Chem. Int. Ed.* **2010,** *49*, 2146-2149.
21. Chockla, A. M.; Klavetter, K. C.; Mullins, C. B.; Korgel, B. A., Tin-Seeded Silicon Nanowires for High Capacity Li-Ion Batteries. *Chem. Mater.* **2012,** *24*, 3738-3745.
22. Chan, C. K.; Patel, R. N.; O'Connell, M. J.; Korgel, B. A.; Cui, Y., Solution-Grown Silicon Nanowires for Lithium-Ion Battery Anodes. *ACS Nano* **2010,** *4*, 1443-1450.
23. Deshpande, R.; Cheng, Y. T.; Verbrugge, M. W., Modeling Diffusion-Induced Stress in Nanowire Electrode Structures. *J. Power Sources* **2010,** *195*, 5081-5088.
24. Chockla, A. M.; Panthani, M. G.; Holmberg, V. C.; Hessel, C. M.; Reid, D. K.; Bogart, T. D.; Harris, J. T.; Mullins, C. B.; Korgel, B. A., Electrochemical Lithiation of Graphene-Supported Silicon and Germanium for Rechargeable Batteries. *J. Phys. Chem. C* **2012**, *116*, 11917-11923.
25. Ruffo, R.; Hong, S. S.; Chan, C. K.; Huggins, R. A.; Cui, Y., Impedance Analysis of Silicon Nanowire Lithium Ion Battery Anodes. *J. Phys. Chem. C* **2009,** *113*, 11390-11398.
26. Luo, J.; Zhao, X.; Wu, J.; Jang, H. D.; Kung, H. H.; Huang, J., Crumpled Graphene-Encapsulated Si Nanoparticles for Lithium Ion Battery Anodes. *J. Phys. Chem. Lett.* **2012,** 3, 1824-1829.
27. Fukui, H.; Ohsuka, H.; Hino, T.; Kanamura, K., A Si-O-C Composite Anode: High Capability and Proposed Mechanism of Lithium Storage Associated with Microstructural Characteristics. *ACS Appl. Mater. Interfaces* **2010,** *2*, 998-1008.

28. Shen, J.; Raj, R., Silicon-Oxycarbide Based Thin Film Anodes for Lithium Ion Batteries. *J. Power Sources* **2011,** *196*, 5945-5950.
29. Ahn, D.; Raj, R., Cyclic Stability and C-Rate Performance of Amorphous Silicon and Carbon Based Anodes for Electrochemical Storage of Lithium. *J. Power Sources* **2011**, *196*, 2179-2186.
30. Bhandavat, R.; Singh, G. Stable and Efficient Li-Ion Battery Anodes Prepared from Polymer-Derived Silicon Oxycarbide-Carbon Nanotube Shell/Core Composites. *J. Phys. Chem. C* **2013**, *117*, 11899-11905.
31. Ahn, D.; Raj, R., Thermodynamic Measurements Pertaining to the Hysteretic Intercalation of Lithium in Polymer-Derived Silicon Oxycarbide. *J. Power Sources* **2010,** *195*, 3900-3906.
32. Feng, Y., Electrochemical Properties of Heat-Treated Polymer-Derived SiCN Anode for Lithium Ion Batteries. *Electrochim. Acta* **2010,** *55*, 5860-5866.
33. Fukui, H.; Ohsuka, H.; Hino, T.; Kanamura, K., Polysilane/Acenaphthylene Blends Toward Si-O-C Composite Anodes for Rechargeable Lithium-Ion Batteries. *J. Electrochem. Soc.* **2011,** *158*, A550-A555.
34. Kaspar, J.; Graczyk-Zajac, M.; Riedel, R., Determination of the Chemical Diffusion Coefficient of Li-ions in Carbon-Rich Silicon Oxycarbide Anodes by Electro-Analytical Methods. *Electrochim. Acta.* **2014**, *115*, 665-670.
35. Liebau-Kunzmann, V.; Fasel, C.; Kolb, R.; Riedel, R., Lithium Containing Silazanes as Precursors for SiCN: Li Ceramics - A Potential Material for Electrochemical Applications. *J. Eur. Ceram. Soc.* **2006,** *26*, 3897-3901.
36. Su, D.; Li, Y. L.; Feng, Y.; Jin, J., Electrochemical Properties of Polymer-Derived SiCN Materials as the Anode in Lithium Ion Batteries. *J. Am. Ceram. Soc.* **2009,** *92*, 2962-2968.
37. Graczyk-Zajac, M.; Mera, G.; Kaspar, J.; Riedel, R., Electrochemical Studies of Carbon-Rich Polymer-Derived SiCN Ceramics as Anode Materials for Lithium-Ion Batteries. *J. Eur. Ceram. Soc.* **2010,** *30*, 3235-3243.
38. Kaspar, J.; Mera, G.; Nowak, A. P.; Graczyk-Zajac, M.; Riedel, R., Electrochemical Study of Lithium Insertion into Carbon-Rich Polymer-Derived Silicon Carbonitride Ceramics. *Electrochim. Acta* **2010,** *56*, 174-182.

39. Tamai, H.; Sugahara, H.; Yasuda, H., Preparation of Carbons from Pitch Containing Polysilane and their Anode Properties for Lithium-Ion Batteries. *J. Mater. Sci. Lett.* **2000,** *19*, 53-56.
40. Bhandavat, R.; Singh, G., Synthesis, Characterization, and High Temperature Stability of Si(B)CN-Coated Carbon Nanotubes Using a Boron-Modified Poly(ureamethylvinyl)Silazane Chemistry. *J. Am. Ceram. Soc.* **2012,** *95*, 1536-1543.
41. Sarkar, S.; Gan, Z.; An, L.; Zhai, L., Structural Evolution of Polymer-Derived Amorphous SiBCN Ceramics at High Temperature. *J. Phys. Chem. C* **2011,** *115*, 24993-25000.
42. Hermann, A. M.; Wang, Y. T.; Ramakrishnan, P. A.; Balzar, D.; An, L. N.; Haluschka, C.; Riedel, R., Structure and Electronic Transport Properties of Si-(B)-C-N Ceramics. *J. Am. Ceram. Soc.* **2001,** *84*, 2260-2264.
43. Riedel, R.; Kienzle, A.; Dressler, W.; Ruwisch, L.; Bill, J.; Aldinger, F., A Silicoboron Carbonitride Ceramic Stable to 2,000 Degrees C. *Nature* **1996,** *382*, 796-798.
44. David, L.; Asok, D.; Singh, G., Synthesis and Extreme Rate Capability of Si–Al–C–N Functionalized Carbon Nanotube Spray-on Coatings as Li-Ion Battery Electrode. *ACS Appl. Mater. Interfaces.* **2014**, *6*, 16056-16064.
45. Zimmermann, A.; Bauer, A.; Christ, M.; Cai, Y.; Aldinger, F., High-Temperature Deformation of Amorphous Si-C-N and Si-B-C-N Ceramics Derived from Polymers. *Acta Mater.* **2002,** *50*, 1187-1196.
46. Ramakrishnan, P. A.; Wang, Y. T.; Balzar, D.; An, L. A.; Haluschka, C.; Riedel, R.; Hermann, A. M., Silicoboron-Carbonitride Ceramics: A Class of High-Temperature, Dopable Electronic Materials. *App. Phys. Lett.* **2001,** *78*, 3076-3078.
47. Bhandavat, R.; Singh, G., Improved Electrochemical Capacity of Precursor-Derived Si(B)CN-Carbon Nanotube Composite as Li-Ion Battery Anode. *ACS Appl. Mater. Interfaces* **2012,** *4*, 5092-5097.
48. Feng, Y.; Du, G. X.; Zhao, X. J.; Yang, E. C., Preparation and Electrochemical Performance of SiCN-CNTs Composite Anode Material for Lithium Ion Batteries. *J Appl. Electrochem.* **2011,** *41*, 999-1002.

49. Graczyk-Zajac, M.; Fasel, C.; Riedel, R., Polymer-Derived-SiCN Ceramic/Graphite Composite as Anode Material with Enhanced Rate Capability for Lithium Ion Batteries. *J. Power Sources* **2011,** *196*, 6412-6418.
50. Kolb, R.; Fasel, C.; Liebau-Kunzmann, V.; Riedel, R., SiCN/C-Ceramic Composite as Anode Material for Lithium Ion Batteries. *J. Eur. Ceram. Soc.* **2006,** *26*, 3903-3908.
51. Bechelany, M.; Bernard, S.; Brioude, A.; Cornu, D.; Stadelmann, P.; Charcosset, C.; Fiaty, K.; Miele, P., Synthesis of Boron Nitride Nanotubes by a Template-Assisted Polymer Thermolysis Process. *J. Phys. Chem. C* **2007**, *111*, 13378-13384.
52. Salles, V.; Bernard, S.; Li, J.; Brioude, A.; Chehaidi, S.; Foucaud, S.; Miele, P., Design of Highly Dense Boron Nitride by the Combination of Spray-Pyrolysis of Borazine and Additive-Free Sintering of Derived Ultrafine Powders. *Chem. Mater.* **2009**, *21*, 2920-2929.
53. Termoss, H.; Toury, B.; Pavan, S.; Brioude, A.; Bernard, S.; Cornu, D.; Valette, S.; Benayoun, S.; Miele, P., Preparation of Boron Nitride-Based Coatings on Metallic Substrates Via Infrared Irradiation of Dip-Coated Polyborazylene. *J. Mater. Chem.* **2009**, *19*, 2671-2674.
54. Li, J.; Bernard, S.; Salles, V.; Gervais, C.; Miele, P., Preparation of Polyborazylene-Derived Bulk Boron Nitride with Tunable Properties by Warm-Pressing and Pressureless Pyrolysis. *Chem. Mater.* **2010**, *22*, 2010-2019.
55. Alauzun, J. G.; Ungureanu, S.; Brun, N.; Bernard, S.; Miele, P.; Backov, R.; Sanchez, C., Novel Monolith-Type Boron Nitride Hierarchical Foams Obtained Through Integrative Chemistry. *J. Mater. Chem.* **2011**, *21*, 14025-14030.
56. Schlienger, S.; Alauzun, J.; Michaux, F.; Vidal, L.; Parmentier, J.; Gervais, C.; Babonneau, F.; Bernard, S.; Miele, P.; Parra, J. B., Micro-, Mesoporous Boron Nitride-Based Materials Templated from Zeolites. *Chem. Mater.* **2012**, *24*, 88-96
57. Zhong, W.; Wang, S.; Li, J.; Bechelany, M. C.; Ghisleni, R.; Rossignol, F.; Balan, C.; Chartier, T.; Bernard, S.; Miele, P., Design of Carbon Fiber Reinforced Boron Nitride Matrix Composites by Vacuum-Assisted Polyborazylene Transfer Molding and Pyrolysis. *J. Eur. Ceram. Soc.* **2013**, *33*, 2979-2992.
58. Hummers, W. S.; Offeman, R. E., Preparation of Graphitic Oxide. *J. Am. Chem. Soc.* **1958**, *80*, 1339-1339.

59. Li, Y. L.; Kroke, E.; Riedel, R.; Fasel, C.; Gervais, C.; Babonneau, F., Thermal Cross-Linking and Pyrolytic Conversion of Poly(Ureamethylvinyl)Silazanes to Silicon-Based Ceramics. *App. Organomet. Chem.* **2001,** *15*, 820-832.
60. Antsiferov, V. N.; Gilyov, V. G.; Karmanov, V. I., IR-Spectra and Phases Structure of Sialons. *Vib. Spectro.* **2002,** *30*, 169-173.
61. Wada, N.; Solin, S. A.; Wong, J.; Prochazka, S., Raman and Ir Absorption Spectroscopic Studies on Alpha, Beta, and Amorphous Si_3N_4. *J. Non-Crystalline Solids* **1981,** *43*, 7-15.
62. Ermer, E.; Ptak, W. S., FTIR Studies of Structural Effects due to Boron Addition in Sintered Silicon Carbide. *Vib. Spectro.* **2002,** *29*, 211-215.
63. Lv, Q.; Cao, C. B.; Li, C.; Zhang, J. T.; Zhu, H. X.; Kong, X.; Duan, X. F., Formation of Crystalline Carbon Nitride Powder by a Mild Solvothermal Method. *J. Mater. Chem.* **2003,** *13*, 1241-1243.
64. Brun, N.; Janot, R.; Sanchez, C.; Deleuze, H.; Gervais, C.; Morcrette, M.; Backov, R., Preparation of $LiBH_4$@carbon Micro-Macrocellular Foams: Tuning Hydrogen Release Through Varying Microporosity. *Energy Environ. Sci.* **2010**, *3*, 824-830.
65. Wang, C.; Li, D.; Too, C. O.; Wallace, G. G. Electrochemical Properties of Graphene Paper Electrodes Used in Lithium Batteries. *Chem. Mater.* **2009,** *21*, 2604.
66. David, L.; Singh, G. Reduced Graphene Oxide Paper Electrode: Opposing Effect of Thermal Annealing on Li and Na Cyclability. *J. Phys. Chem. C* **2014,** *118*, 28401-28408.
67. Yu, P.; Popov, B. N.; Ritter, J. A.; White, R. E. Determination of the Lithium Ion Diffusion Coefficient in Graphite. *J. Electrochem. Soc.* **1999**, *146*, 8-14.
68. Persson, K.; Sethuraman, V. A.; Hardwick, L. J.; Hinuma, Y.; Meng, Y. S.; Ven, A.; Srinivasan, V.; Kostecki, R.; Ceder, G. Lithium Diffusion in Graphitic Carbon. *J. Phys. Chem. Lett.* **2010**, *1*, 1176– 1180.

FIGURES

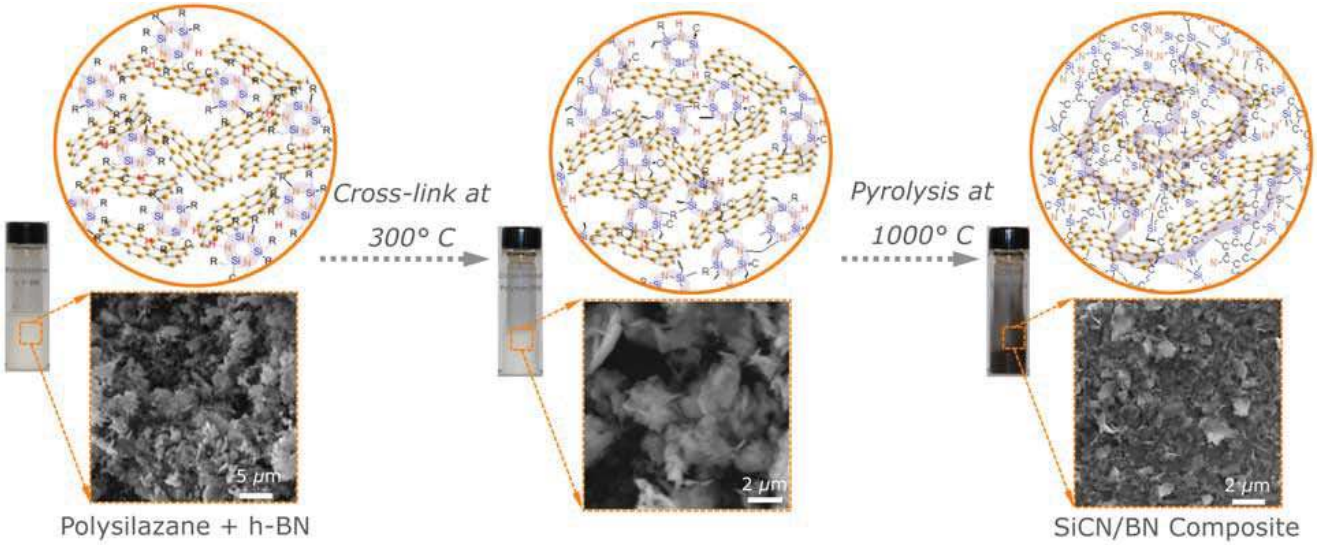

FIGURE 1. Schematic showing polymer to ceramic conversion and simultaneous incorporation of BN sheets in SiCN matrix. (L to R): polysilazane precursor uniformly wets BN sheets when they are stirred together. As the mixture is heated in flowing N_2, polysilazane cross-links at approximately 300 °C to form long chains connected by BN sheets. Further pyrolysis at 1000 °C forms BN sheets embedded with SiCN ceramic matrix. Inset shows SEM images of composite at various stages of processing.

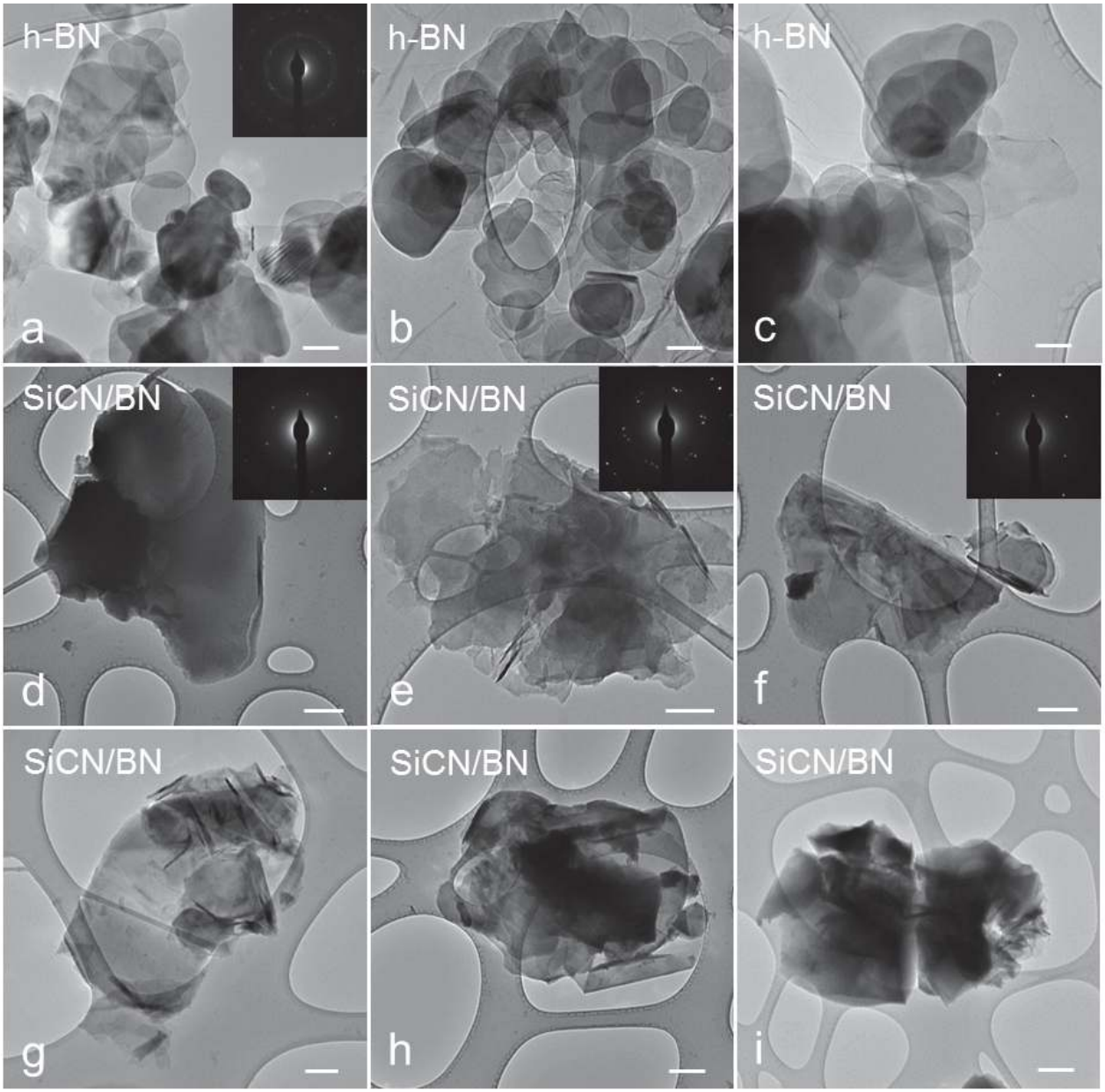

FIGURE 2. (a through c): TEM images of as-obtained BN sheets, (d through i): as-synthesized SiCN/BN composite material. The insets show the SAED pattern obtained for the corresponding TEM image. SiCN/BN showed distinct pattern corresponding to BN. Scale bar is 50 nm.

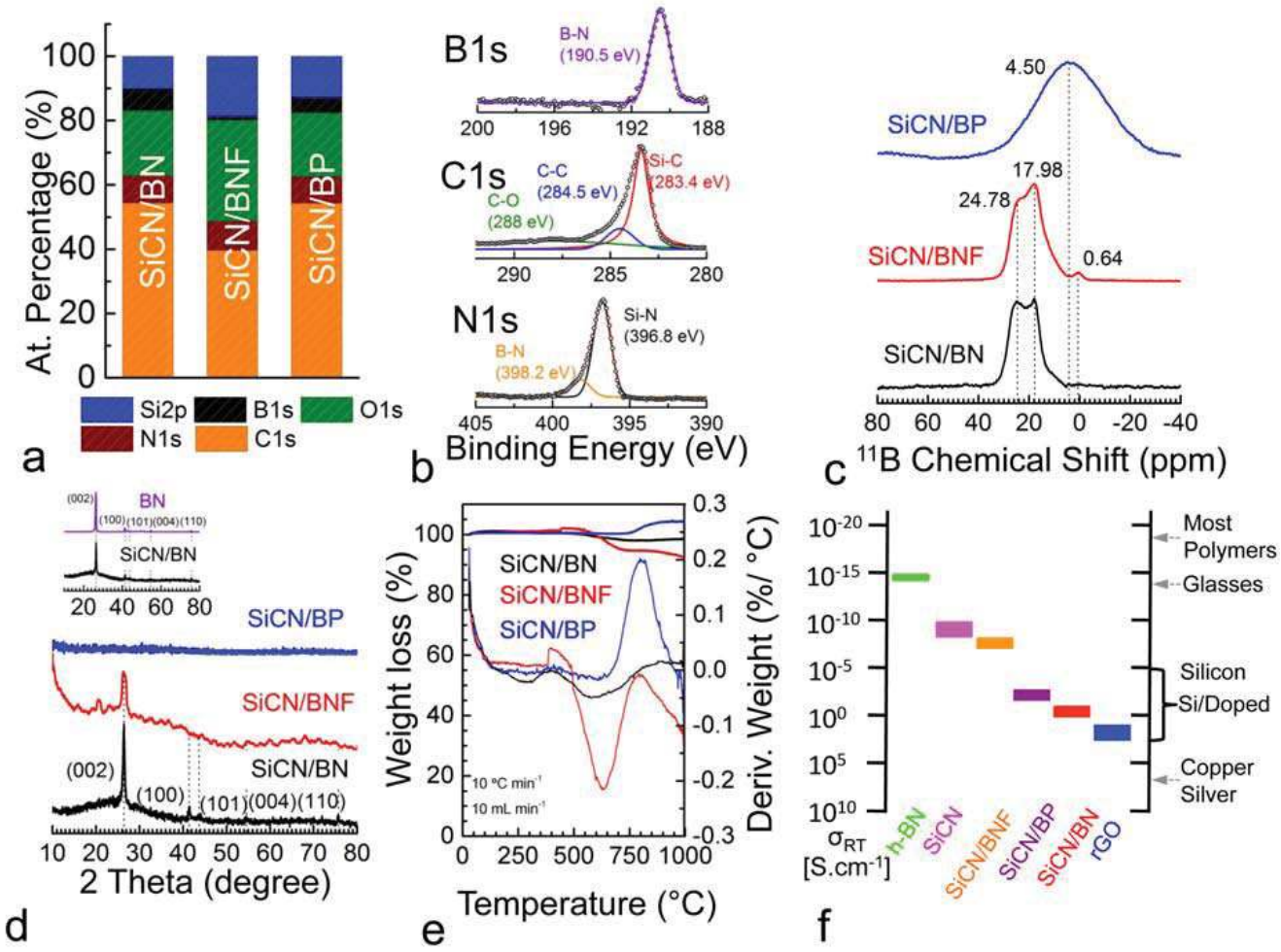

FIGURE 3. (a) Bar chart of atomic percentage of elements present in SiCN/BN, SiCN/BNF and SiCN/BP composites obtained using XPS. (b) High-resolution XPS of B 1s, C 1s and N 1s peaks in SiCN/BN composites. (c) ^{11}B NMR spectra showing B-N bonds in planar BN_3 groups in case of SiCN/BN and SiCN/BNF and amorphous boron in SiCN/BP ceramic composites. (d) XRD comparison SiCN/BN, SiCN/BNF and SiCN/BP composites. Inset shows X-ray comparison of 'as-obtained' BN powder and SiCN/BN composite. Characteristic BN peaks were clearly observed in SiCN/BN composite. (e) Thermogravimetric analysis plots of three composites proving SiCN/BN's high thermal stability and oxidation resistance. (f) Electrical conductivity comparison of various SiCN PDCs specimen prepared in this study. rGO and BN are included to demonstrate the wide range in conductivity that can be achieved in these ceramics.

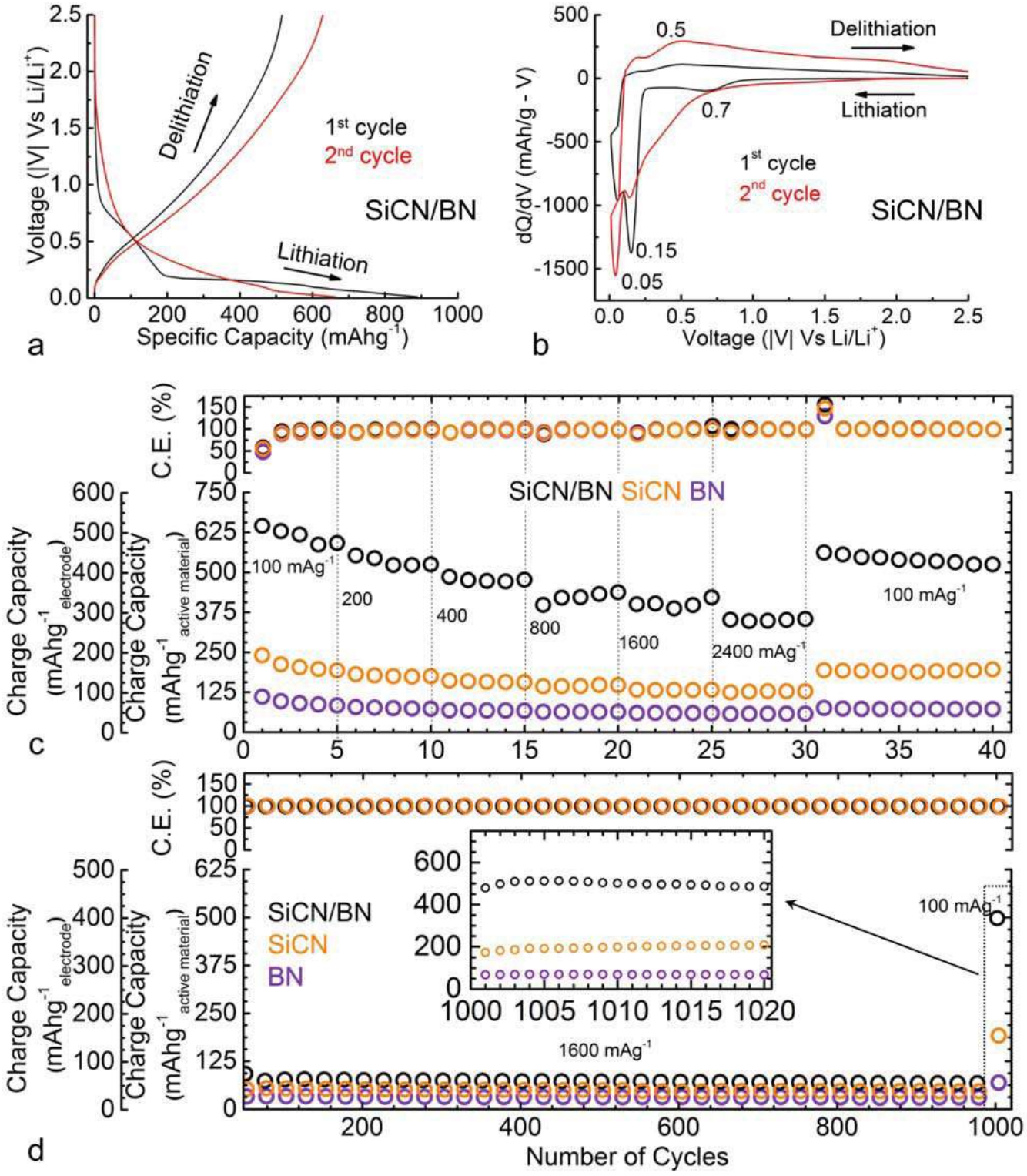

FIGURE 4. 1st and 2nd cycle (a) voltage profile and (b) differential capacity curve of SiCN/BN/rGO. (c) Charge capacity of SiCN/BN/rGO with BN/rGO and SiCN/rGO for comparison. Cells were cycled asymmetrically at increasing rates for every five cycles. (d)

Charge capacity when symmetrically at 1600 mA g^{-1} for 1000 cycles and return to 100 mA g^{-1}. Charge capacity of SiCN/BN was more than twice than the capacity of SiCN.

TABLE 1 Summary of electrochemical cycling data for various electrodes used in this study and comparison with data from literature. *NOTE: All electrodes in the present study were prepared with approximately 20 wt % rGO. Capacity values are with respect to total electrode weight.*

Electrode material	1st Cycle charge, mAh g^{-1}	Capacity at max. current density tested, mAh g^{-1}	Max. number of cycles tested	Charge capacity after 1000 cycles at 100 mA g^{-1}
SiCN/BN	475 ±42 *	283.2 (2400)	1020	400.8
SiCN/BNF	262.4	100.8 (2400)	1020	202.4
SiCN/BP	140	68.8 (2400)	1020	95.2
SiCN	192	102.3 (2400)	1020	159.2
BN	88.8	46.4 (2400)	1020	55.2
BP	99.2	55.2 (2400)	1020	68
SiCN-1000 °C [36]	456	171 (100)	30	-
SiCN-1100 °C[37]	263	100 (36)	50	-
SiCN-1300 °C/O_2 [37]	291	250 (72)	60	-
SiCN-1100 °C[38]	254	95 (360)	10	-
Si(B)CN-CNT[47]	362	430 (100)	30	-
SiCN-Graphene[49]	420	440 (40)	50	-
Graphite[65]	298	240 (50)	50	-
rGO-500 °C[66]	292	180 (2400)	1020	190

** Average of three samples. Refer supporting Information Figure S11*

TOC GRAPHICS